Massive MIMO Indoor Localization with 64-Antenna Uniform Linear Array

Bin Liu, Andrea P. Guevara, Sibren De Bast, Qing Wang, and Sofie Pollin
Department of Electrical Engineering, KU Leuven, Belgium.
Email: {bin.liu, andrea.guevara, sibren.debast, qing.wang, sofie.pollin}@esat.kuleuven.be

***Abstract*—Localization is crucial for nowadays' communication systems, especially for beamforming techniques in massive MIMO systems. Large-scale MIMO systems have exhibited their advantages in communications. In the meantime, they also have the potential to provide accurate localization with their high angular resolution. In this paper, we study indoor localization performance of a Massive MIMO system with a 64-antenna Uniform Linear Array (ULA). Based on the sparse reconstruction method, we propose a Mixed field Sparse Bayesian Learning (MSBL) algorithm to localize devices for both near-field and far-field scenarios. Using the measurement results from our massive MIMO testbed, we show that our proposed MSBL algorithm can improve the localization accuracy by 49% with only a few snapshots. The performance of our algorithm is also robust to low Signal-to-Noise Ratio (SNR) conditions.**

I. Introduction

Indoor localization is enabling a manifold of promising applications, such as navigation in smart buildings and factories and more secure distributed Internet of Things (IoT) [1], among others. In future wireless communication networks, there is a trend to integrate communication, localization, sensing, and mapping into a single system. This system will leverage the deployment of massive amounts of antennas to provide multiple services.

Motivation. From the communication aspect, the fascination of massive Multiple-Input Multiple-Output (MIMO) systems is the harvested antenna diversity gain by beamforming, whose performance relies on the accurate channel estimation and the localization of User Equipment (UE). Regarding localization, the large numbers of antennas in massive MIMO systems can reap high angular resolution [2], especially when arranging the antennas in a Uniform Linear Array (ULA).

Challenges. In this paper we study indoor localization in a massive MIMO system with a ULA antenna topology, as shown in Fig. 1(a). There are mainly two challenges: *(i)* In contrast to outdoor scenarios where localization can reap the benefits of Line-of-Sight (LoS) links, the multipath effects of the radio waves in indoor scenarios generate more spurious signals when estimating the positions of UEs; *(ii)* The Fraunhofer distance $d_F = 2D^2/\lambda$ is related to the dimension of the antenna array, where D is the array length and λ is the signal wavelength. This means increasing the number of antennas changes the electromagnetic radiation from far-field to near-field. Without the prior knowledge of a UE's position, it is hard to classify the localization problem with the correct radiation scenario. Furthermore, the localization algorithm should be able to handle both far-field and near-field scenarios.

(a) ULA: Uniform Linear Array (b) UPA: Uniform Planar Array

Fig. 1: Massive MIMO system with different antenna arrays

Contributions. We summarize our contributions as follows:

- *Mixed near-field and far-field localization.* We estimate the position of the UE with Mixed field Sparse Bayesian Learning (MSBL) algorithm. Without prior position knowledge, MSBL can localize the UE for both near-field and far-field scenarios with high accuracy.
- *Does angular resolution increase with the number of antennas?* We measure the indoor scenario channel with a real-time massive MIMO testbed operating at 2.61 GHz, and verify the relationships between the number of antennas and angular resolution under far-field and near-field scenarios.
- *Directional or omnidirectional antenna?* Capable of radiating electro-magnetic power in all directions, the omnidirectional dipole antenna nevertheless generates a more spurious signal, and intuitively decays the estimation accuracy. In this paper, we measure the channel separately with a directional patch antenna and an omnidirectional dipole antenna at the UE, and quantify the performance difference. Based on sparse reconstruction, the proposed MSBL algorithm can narrow this performance gap.

II. System Model

Consider that K narrow-band signals from UEs parameterized by (θ_k, r_k), $k = 1, 2, \ldots, K$, impinge on a symmetric uniform linear array with M antennas, where θ_k and r_k represent the angel of arrival and transmission path length of the signal from k-th UE. The antennas of the ULA are indexed by $\{1, 2 \ldots, M\}$ from the left to right, and the antenna spacing

$$\boldsymbol{a}_F(\theta_k) = \left[1, \exp\left(-\mathrm{j}\frac{2\pi d \sin\theta_k}{\lambda}\right), \cdots, \exp\left(-\mathrm{j}\frac{2\pi(M-1)d\sin\theta_k}{\lambda}\right)\right]^{\mathrm{T}}, \ k = 1, 2, \cdots, K_1, \tag{7}$$

$$\boldsymbol{a}_N(r_k, \theta_k) \approx \left\{1, \cdots, \exp\left[\mathrm{j}\left(m\alpha_k + m^2\beta_k\right)\right], \cdots, \exp\left[\mathrm{j}\left((M-1)\alpha_k + (M-1)^2\beta_k\right)\right]\right\}^{\mathrm{T}}, \ k = K_1+1, \cdots, K. \tag{8}$$

in the array is d. With the 1-st antenna as the reference point, the received signal at the m-th antenna can be modeled as

$$x_m(t) = \sum_{k=1}^{K} s_k(t - \tau_{mk}) + n_m(t), \tag{1}$$

where $s_k(t)$ is the k-th signal and $n_m(t)$ is the additive noise. τ_{mk} is the phase shift by the k-th signal's propagation time delay from the reference point to the m-th antenna, which is in the form of

$$\tau_{mk} = \frac{2\pi}{\lambda}\left(\sqrt{r_k^2 + ((m-1)d)^2 - 2r_k(m-1)d\sin\theta_k} - r_k\right), \tag{2}$$

where λ is the wavelength of the UEs' signal wavefronts.

In this paper, we consider both the near-field and far-field localization problem, without priori knowledge of the UEs' positions. For a far-field UE, the transmission path is much larger than the array aperture size, therefore, the wavefront approximates to a plane wave and the propagation time delay τ_{mk} is approximated by [3]

$$\tau_{mk} \approx -\frac{2\pi(m-1)d}{\lambda}\sin\theta_k. \tag{3}$$

For a near-field occasion, i.e., the UE is in the Fresnel zone of the array, transmission path r_k is on the order of only a few array apertures. The amplitudes of the received signals' envelopes at each antenna are approximately the same, and thus the wavefronts are in the form of spherical wave. With the Frenel approximation [3], the propagation time delay τ_{mk} can be approximated by the Taylor expansion of (2)

$$\begin{aligned}\tau_{mk} &\approx -\frac{2\pi}{\lambda}(m-1)d\sin\theta_k + \frac{\pi((m-1)d)^2}{\lambda r_k}\cos^2\theta_k \\ &= (m-1)\alpha_k + (m-1)^2\beta_k,\end{aligned} \tag{4}$$

where α_k and β_k are defined as electric angles, and we have

$$\alpha_k = -\frac{2\pi d}{\lambda}\sin\theta_k, \qquad \beta_k = \frac{\pi d^2}{\lambda r_k}\cos^2\theta_k. \tag{5}$$

Note that, as observed in (5), as r_k approaches to $+\infty$, the far-field UE can be deemed as a limiting case of the near-field one. Assume that K narrow-band UEs contain K_1 far-field signals and $K - K_1$ near-field signals, and whose transmit signal vectors are denoted by $\boldsymbol{s}_F(t) = [s_1(t), \cdots, s_{K_1}(t)]^{\mathrm{T}}$ and $\boldsymbol{s}_N(t) = [s_{K_1+1}(t), \cdots, s_K(t)]^{\mathrm{T}}$. In vector form, we have

$$\boldsymbol{x}(t) = \begin{bmatrix} \boldsymbol{A}_F(\boldsymbol{\theta}) & \boldsymbol{A}_N(\boldsymbol{r}, \boldsymbol{\theta}) \end{bmatrix} \begin{bmatrix} \boldsymbol{s}_F(t) \\ \boldsymbol{s}_N(t) \end{bmatrix} + \boldsymbol{n}(t), \tag{6}$$

where $\boldsymbol{n}(t) = [n_1(t), \cdots, n_m(t)]^{\mathrm{T}}$ is zero-mean, additive white Gaussian noise with power σ^2, which is statistically independent of all impinging UEs' signals. The array steering matrix for far-field and near-field UEs are denoted by $\boldsymbol{A}_F(\boldsymbol{\theta}) = [\boldsymbol{a}_F(\theta_1), \cdots, \boldsymbol{a}_F(\theta_{K_1})]$ and $\boldsymbol{A}_N(\boldsymbol{\theta}) = [\boldsymbol{a}_N(r_{K_1+1}, \theta_{K_1+1}), \cdots, \boldsymbol{a}_N(r_K, \theta_K)]$, respectively, and steering vectors have the form as shown in Eq. (7) and Eq. (8).

Let us divide the total angle range $(-90°, 90°)$ into N discrete angles, e.g., $\boldsymbol{\Theta} = \{\theta_1, \cdots, \theta_n \cdots, \theta_N\}$, $1 \leqslant n \leqslant N$, where $\theta_n = -90° + \frac{n-1}{N}180°$, and let us discretize the path length by 0.1λ similarly into $r_1, r_2, \cdots, r_V$, e.g., $(\boldsymbol{R}, \boldsymbol{\Theta}) = \{(r_1, \theta_1), \cdots, (r_v, \theta_n), \cdots, (r_V, \theta_N)\}$. Then, we have a discrete array matrix as

$$\boldsymbol{A} = \begin{bmatrix} \boldsymbol{A}_F(\boldsymbol{\Theta}) & \boldsymbol{A}_N(\boldsymbol{R}, \boldsymbol{\Theta}) \end{bmatrix}. \tag{9}$$

Consider L snapshots that are collected at the antenna array, $\boldsymbol{X} = [\boldsymbol{x}(t_1), \cdots, \boldsymbol{x}(t_L)] \in \mathbb{C}^{M\times L}$, and the expression for multiple snapshots is formed as

$$\boldsymbol{X} = \boldsymbol{A}\boldsymbol{S} + \boldsymbol{N}, \tag{10}$$

where we vectorize the transmit signal and noise as the $\boldsymbol{S} = [s(t_1), \cdots, s(t_L)] \in \mathbb{C}^{N\times L}$ and $\boldsymbol{N} = [\boldsymbol{n}(t_1), \cdots, \boldsymbol{n}(t_L)] \in \mathbb{C}^{M\times L}$, respectively. The received signal matrix is sparse and underdetermined due to the following facts, a) the number of UEs is less than the number of antennas in the array, i.e., $K \ll M$, b) to achieve spatial resolution, the sampling interval is usually small, and thus there are only a few nonzero rows in the signal matrix $\boldsymbol{S}$. The signal vector at the UE $\boldsymbol{s}_l$ is K-sparse, and $K \ll N$. We define the l-th active set

$$\mathcal{N}_l = \{n \in \mathbb{N} | x_{nl} \neq 0\} = \{n_1, n_2, \ldots, n_K\}, \tag{11}$$

and assume $\mathcal{N}_l = \mathcal{N}$ is constant across snapshots l. Also, we define $\boldsymbol{A}_{\mathcal{N}} \in \mathbb{C}^{M\times K}$ which only contains K active columns of $\boldsymbol{A}$.

With (10), the localization problem can be formulated as the fitting problem that finds K basis functions from the overcomplete dictionary $\boldsymbol{A}$ to match the $\boldsymbol{X}$ and $\boldsymbol{A}\boldsymbol{S}$. From K selected basis functions in $\boldsymbol{A}$, i.e., $\boldsymbol{A}_{\mathcal{N}}$, we can deduce the location information, such as the angle of arrival and the path length. With the sparse model, the objective function can be expressed as

$$\mathcal{L}(\boldsymbol{S}|\boldsymbol{X}) = \|\boldsymbol{X} - \boldsymbol{A}\boldsymbol{S}\|_F^2 + \beta\mathcal{G}(\boldsymbol{S}), \tag{12}$$

where $\|\boldsymbol{X} - \boldsymbol{A}\boldsymbol{S}\|_F^2$ represents the error of fitting between the observed signal and the signal generated by the sparse model. $\mathcal{G}(\boldsymbol{S})$ is the penalty function and used for the sparsity constraint of $\boldsymbol{S}$. β consist of regularized factors, and embodies the trade-off between the error of fitting and sparsity.

III. Proposed Learning Method for Localization

In this section, we solve the mixed field localization problem with sparse Bayesian learning [4] and Maximum-A-Posteriori (MAP) is used for the reconstruction of the angle of arrival. The likelihood and prior information are assumed as complex Gaussian distributions with unknown variances (hyperparameters). By maximizing the Type-II likelihood (evidence) for Gaussian signals hidden in Gaussian noise, we can determine the hyperparameters with stochastic maximum likelihood [5], [6] in the estimation.

A. Likelihood

With the assumption that the observed noise in (10) is complex Gaussian, the conditional Probability Density Function (PDF) for the single-frequency signal observations $\boldsymbol{X}$ is also complex Gaussian with noise variance σ^2.

$$p\left(\boldsymbol{X}|\boldsymbol{S};\sigma^2\right)=\frac{\exp\left(-\frac{1}{\sigma^2}\|\boldsymbol{X}-\boldsymbol{A}\boldsymbol{S}\|_{\mathcal{F}}^2\right)}{\left(\pi\sigma^2\right)^{KL}}, \tag{13}$$

where $\boldsymbol{S}$ is the UEs' transmit signal, which gives the signal observations $\boldsymbol{X}$.

B. Prior

Let $\boldsymbol{s}_l$ denote the UE signal vector for the l-th observation (snapshot), $l\in[1,\cdots,L]$, whose elements s_{nl} have complex amplitudes with angle θ_n at the l-th observation. It is found that it is independent with snapshots l and angles θ_n, and follows a zero-mean complex Gaussian distribution with angle of arrival dependent variance $\gamma_n\in\boldsymbol{\gamma}=[\gamma_1,\ldots,\gamma_N]^T$,

$$p_n\left(s_{nl};\gamma_n\right)=\begin{cases}\delta\left(s_{nl}\right), & \text{for } \gamma_n=0\\ \frac{1}{\pi\gamma_n}\mathrm{e}^{-|s_{nl}|^2/\gamma_n}, & \text{for } \gamma_n>0\end{cases}, \tag{14}$$

$$p(\boldsymbol{S};\boldsymbol{\gamma})=\prod_{l=1}^{L}\prod_{n=1}^{N}p_n\left(s_{nl};\gamma_n\right)=\prod_{l=1}^{L}\mathcal{CN}(\boldsymbol{0},\boldsymbol{\Gamma}), \tag{15}$$

From (15), the UE signal vector $\boldsymbol{s}_l$ has a multivariate Gaussian distribution with a potentially singular covariance matrix,

$$\boldsymbol{\Gamma}=\mathrm{diag}(\boldsymbol{\gamma})=\mathrm{E}\left[\boldsymbol{s}_l\boldsymbol{s}_l^H;\boldsymbol{\gamma}\right], \tag{16}$$

as $\mathrm{rank}(\boldsymbol{\Gamma})=E\leq M$. Note that the diagonal elements of $\boldsymbol{\Gamma}$, i.e., the hyperparameters $\boldsymbol{\gamma}\geq 0$ represent the UE signal powers. The variance γ_m is zero only when x_{nl} is zero. The hyperparameter $\boldsymbol{\gamma}$ determines the sparsity of the model.

C. Posterior

By Bayes rule conditioned on $\boldsymbol{\gamma}$, σ^2, the posterior PDF for the UE signals' amplitudes $\boldsymbol{S}$ is

$$p\left(\boldsymbol{S}|\boldsymbol{X};\boldsymbol{\gamma},\sigma^2\right)\equiv\frac{p\left(\boldsymbol{X}|\boldsymbol{S};\sigma^2\right)p(\boldsymbol{S};\boldsymbol{\gamma})}{p\left(\boldsymbol{X};\boldsymbol{\gamma},\sigma^2\right)}, \tag{17}$$

where denominator $p\left(\boldsymbol{X};\boldsymbol{\gamma},\sigma^2\right)$ is the evidence term

$$\begin{aligned}&p\left(\boldsymbol{S}|\boldsymbol{X};\boldsymbol{\gamma},\sigma^2\right)\propto p\left(\boldsymbol{X}|\boldsymbol{S};\sigma^2\right)p(\boldsymbol{S};\boldsymbol{\gamma})\\ &\propto\frac{\mathrm{e}^{-\mathrm{tr}\left((\boldsymbol{S}-\boldsymbol{\mu}_{\boldsymbol{S}})^H\boldsymbol{\Sigma}_s^{-1}(\boldsymbol{S}-\boldsymbol{\mu}_{\boldsymbol{S}})\right)}}{\left(\pi^N\det\boldsymbol{\Sigma}_s\right)^L}=\mathcal{CN}\left(\boldsymbol{\mu}_{\boldsymbol{S}},\boldsymbol{\Sigma}_{\boldsymbol{s}}\right).\end{aligned} \tag{18}$$

As $p\left(\boldsymbol{X}|\boldsymbol{S};\sigma^2\right)$ and $p(\boldsymbol{S};\boldsymbol{\gamma})$ are Gaussians, their product in (18) is Gaussian with posterior mean $\boldsymbol{\mu}_{\boldsymbol{S}}$ and covariance $\boldsymbol{\Sigma}_{\boldsymbol{s}}$, where

$$\boldsymbol{\mu}_{\boldsymbol{S}}=\mathrm{E}\left\{\boldsymbol{S}|\boldsymbol{X};\boldsymbol{\gamma},\sigma^2\right\}=\boldsymbol{\Gamma}\boldsymbol{A}^H\Sigma_{\boldsymbol{x}}^{-1}\boldsymbol{X}, \tag{19}$$

$$\begin{aligned}\boldsymbol{\Sigma}_{\boldsymbol{s}}&=\mathrm{E}\left\{\left(\boldsymbol{s}_l-\boldsymbol{\mu}_{\boldsymbol{s}_l}\right)\left(\boldsymbol{s}_l-\boldsymbol{\mu}_{\boldsymbol{s}_l}\right)^H|\boldsymbol{X};\boldsymbol{\gamma},\sigma^2\right\}\\ &=\left(\frac{1}{\sigma^2}\boldsymbol{A}^H\boldsymbol{A}+\boldsymbol{\Gamma}^{-1}\right)^{-1}=\boldsymbol{\Gamma}-\boldsymbol{\Gamma}\boldsymbol{A}^H\Sigma_{\boldsymbol{x}}^{-1}\boldsymbol{A}\boldsymbol{\Gamma}\end{aligned}, \tag{20}$$

where the array data covariance $\Sigma_{\boldsymbol{x}}$ and its inverse has form

$$\boldsymbol{\Sigma}_{\boldsymbol{x}}=\mathrm{E}\left\{\boldsymbol{x}_l\boldsymbol{x}_l^H\right\}=\sigma^2\boldsymbol{I}_N+\boldsymbol{A}\boldsymbol{\Gamma}\boldsymbol{A}^H, \tag{21}$$

$$\begin{aligned}\boldsymbol{\Sigma}_{\boldsymbol{x}}^{-1}&=\sigma^{-2}\boldsymbol{I}_N-\sigma^{-2}\boldsymbol{A}\left(\frac{1}{\sigma^2}\boldsymbol{A}^H\boldsymbol{A}+\boldsymbol{\Gamma}^{-1}\right)^{-1}\boldsymbol{A}^H\sigma^{-2}\\ &=\sigma^{-2}\boldsymbol{I}_N-\sigma^{-2}\boldsymbol{A}\boldsymbol{\Sigma}_{\boldsymbol{s}}\boldsymbol{A}^H\sigma^{-2}.\end{aligned} \tag{22}$$

If $\boldsymbol{\gamma}$ and σ^2 are known then the MAP estimate is the posterior mean,

$$\hat{\boldsymbol{S}}^{\mathrm{MAP}}=\boldsymbol{\mu}_{\boldsymbol{S}}=\boldsymbol{\Gamma}\boldsymbol{A}^H\boldsymbol{\Sigma}_{\boldsymbol{x}}^{-1}\boldsymbol{X}, \tag{23}$$

The diagonal elements of $\boldsymbol{\gamma}$ control the row-sparsity of $\hat{\boldsymbol{S}}^{\mathrm{MAP}}$ as for $\gamma_m=0$ the corresponding n-th row of $\hat{\boldsymbol{S}}^{\mathrm{MAP}}$ becomes $\boldsymbol{0}^{\mathrm{T}}$. Thus, the active set $\mathcal{N}$ is equivalently defined by

$$\mathcal{N}=\left\{n\in\mathbb{N}|\gamma_n>0\right\}. \tag{24}$$

D. Evidence

The hyperparameters $\boldsymbol{\gamma}$, σ^2 in (20)-(22),

$$\begin{aligned}p\left(\boldsymbol{X};\boldsymbol{\gamma},\sigma^2\right)&=\int_{\mathbb{R}^{2NL}}p\left(\boldsymbol{X}|\boldsymbol{S};\sigma^2\right)p(\boldsymbol{S};\boldsymbol{\gamma})\mathrm{d}\boldsymbol{S}\\ &=\frac{\mathrm{e}^{-\mathrm{tr}\left(\boldsymbol{X}^H\boldsymbol{\Sigma}_x^{-1}\boldsymbol{X}\right)}}{\left(\pi^N\det\boldsymbol{\Sigma}_{\boldsymbol{x}}\right)^L},\end{aligned} \tag{25}$$

where $\mathrm{d}\boldsymbol{S}=\prod_{l=1}^{L}\prod_{n=1}^{N}\mathrm{Re}\left(\mathrm{d}S_{nl}\right)\mathrm{Im}\left(\mathrm{d}S_{nl}\right)$, and $\boldsymbol{\Sigma}_{\boldsymbol{x}}$ is the received signal covariance. The L-snapshot marginal loglikelihood is rewritten as

$$\log p\left(\boldsymbol{X};\boldsymbol{\gamma},\sigma^2\right)\propto-\mathrm{tr}\left(\boldsymbol{\Sigma}_{\boldsymbol{x}}^{-1}\boldsymbol{S}_{\boldsymbol{x}}\right)-\log\det\boldsymbol{\Sigma}_{\boldsymbol{x}}, \tag{26}$$

where we define the data sample covariance matrix

$$\boldsymbol{R}_{\boldsymbol{x}}=\boldsymbol{X}\boldsymbol{X}^H/L. \tag{27}$$

Note that (27) does not involve the inverse of $\boldsymbol{R}_{\boldsymbol{x}}$ hence it works well even for only few snapshots (small L). The hyperparameters $\boldsymbol{\gamma}$, σ^2 are obtained by maximizing the evidence

$$\left(\hat{\gamma},\hat{\sigma}^2\right)=\underset{\boldsymbol{\gamma}\geq 0,\sigma^2>0}{\arg\max}\log p\left(\boldsymbol{X};\boldsymbol{\gamma},\sigma^2\right). \tag{28}$$

E. UE transmit power estimation

The derivative of (26) is

$$\frac{\partial\log p\left(\boldsymbol{X};\boldsymbol{\gamma},\sigma^2\right)}{\partial\gamma_n}=\frac{1}{\gamma_n^2L}\|\boldsymbol{\mu}_n\|_2^2-\boldsymbol{a}_n^H\boldsymbol{\Sigma}_{\boldsymbol{x}}^{-1}\boldsymbol{a}_n, \tag{29}$$

Algorithm 1 Mixed Field Multiple-Snapshot Sparse Bayesian Learning Algorithm

Input: $\boldsymbol{A} \in \mathbb{C}^{M\times N}, \quad \boldsymbol{X} \in \mathbb{C}^{M\times L}, \quad K$
Initialize: $\sigma_0^2 = 0.1, \gamma_0 = 1, \epsilon_{\min} = 0.001, j_{\max} = 500$
Set $j = 0, \sigma^2 = \sigma_0^2, \boldsymbol{\gamma} = \gamma_0$
while $\epsilon \geq \epsilon_{\min}$ and $j < j_{\max}$ **do**
  $j = j + 1, \quad \gamma^{\text{old}} = \boldsymbol{\gamma}^{\text{new}}, \quad \boldsymbol{\Gamma} = \text{diag}\left(\boldsymbol{\gamma}^{\text{new}}\right)$
  $\boldsymbol{\Sigma_x} = \text{E}\left\{\boldsymbol{x}_l \boldsymbol{x}_l^H\right\} = \sigma^2 \boldsymbol{I}_N + \boldsymbol{A}\boldsymbol{\Gamma}\boldsymbol{A}^H$
  $\boldsymbol{\mu}_n = \gamma_n \boldsymbol{a}_n^H \boldsymbol{\Sigma}_{\boldsymbol{x}}^{-1} \boldsymbol{X}$
  $\gamma_n^{\text{new}} = \frac{1}{L}\left\|\boldsymbol{\mu}_n\right\|_2^2 + \left(\boldsymbol{\Sigma_s}\right)_{nn}$
  Collect K largest peak of $\boldsymbol{\gamma}$ into the set $\mathcal{N} = \{n_1, \cdots, n_K\}$
  Extract the K active vectors from $\boldsymbol{A}$ into $\boldsymbol{A}_{\mathcal{N}} = \{\boldsymbol{a}_1, \cdots, \boldsymbol{a}_{n_K}\}$
  Update $\left(\sigma^2\right)^{\text{new}} = \frac{1}{M-K}\,\text{tr}\left(\left(\boldsymbol{I}_M - \boldsymbol{A}_{\mathcal{N}}\boldsymbol{A}_{\mathcal{N}}^{+}\right)\boldsymbol{R_x}\right)$.

  $\epsilon = \left\|\boldsymbol{\gamma}^{\text{new}} - \boldsymbol{\gamma}^{\text{old}}\right\|_1 / \left\|\boldsymbol{\gamma}^{\text{old}}\right\|_1$.
end while
Output: $\mathcal{N}$, γ_n^{new}, $\left(\sigma^2\right)^{\text{new}}$.

where $\boldsymbol{\mu}_n = \gamma_n \boldsymbol{a}_n^H \boldsymbol{\Sigma}_{\boldsymbol{x}}^{-1} \boldsymbol{X}$ is the n-th row of $\boldsymbol{\mu}_S$ in (19). With the EM approach [4], we update of γ_n

$$\gamma_n^{\text{new}} = \frac{1}{L}\left\|\boldsymbol{\mu}_n\right\|_2^2 + \left(\boldsymbol{\Sigma_s}\right)_{nn}. \tag{30}$$

F. Noise variance

Let $\boldsymbol{\Gamma}_{\mathcal{N}} = \text{diag}(\boldsymbol{\gamma}_{\mathcal{N}}^{\text{new}})$ denote the covariance matrix of the K active UEs obtained above by corresponding active steering matrix $\boldsymbol{A}_{\mathcal{N}}$ which maximizes (26). The corresponding received signal covariance matrix is

$$\boldsymbol{\Sigma_x} = \sigma^2 \boldsymbol{I}_M + \boldsymbol{A}_{\mathcal{N}}\boldsymbol{\Gamma}_{\mathcal{N}}\boldsymbol{A}_{\mathcal{N}}^H, \tag{31}$$

where $\boldsymbol{I}_M$ is the identity matrix of order M. From Jaffer's necessary condition, the optimal solution $(\boldsymbol{\gamma}_{\mathcal{N},\sigma^2})$ satisfies

$$\boldsymbol{A}_{\mathcal{N}}^H \left(\boldsymbol{R_x} - \boldsymbol{\Sigma_x}\right)\boldsymbol{A}_{\mathcal{N}} = \boldsymbol{0}. \tag{32}$$

Substituting (31) into (32) gives

$$\boldsymbol{A}_{\mathcal{N}}^H \left(\boldsymbol{R}_x - \sigma^2 \boldsymbol{I}_M\right)\boldsymbol{A}_{\mathcal{N}} = \boldsymbol{A}_{\mathcal{N}}^H \boldsymbol{A}_{\mathcal{N}}\boldsymbol{\Gamma}_{\mathcal{N}}\boldsymbol{A}_{\mathcal{N}}^H \boldsymbol{A}_{\mathcal{N}}. \tag{33}$$

Multiplying (32) from right and left with the pseudo inverse $\boldsymbol{A}_{\mathcal{N}}^{+} = \left(\boldsymbol{A}_{\mathcal{N}}^H \boldsymbol{A}_{\mathcal{N}}\right)^{-1} \boldsymbol{A}_{\mathcal{N}}^H$ and $\boldsymbol{A}_{\mathcal{N}}^{+\,H}$ respectively and subtracting $\boldsymbol{R}_x$ from both sides yield,

$$\left(\sigma^2\right)^{\text{new}} = \frac{1}{M-K}\,\text{tr}\left(\left(\boldsymbol{I}_M - \boldsymbol{A}_{\mathcal{N}}\boldsymbol{A}_{\mathcal{N}}^{+}\right)\boldsymbol{R_x}\right). \tag{34}$$

The estimate condition is the sparsity property, i.e., $K < M$.

With received signal $\boldsymbol{X}$ from in the measurement, we can update iteratively $\boldsymbol{\mu_S}$ by (19) and $\boldsymbol{\Sigma_x}$ by (21) with the current $\boldsymbol{\gamma}$. γ_n is updated with (30), and then (34) is used to estimate σ^2. Following the Bayesian learning [5], the algorithm is summarized in Table I. The stop condition is $\epsilon \leq \epsilon_{\min}$, where

$$\epsilon = \left\|\boldsymbol{\gamma}^{\text{new}} - \boldsymbol{\gamma}^{\text{old}}\right\|_1 / \left\|\boldsymbol{\gamma}^{\text{old}}\right\|_1. \tag{35}$$

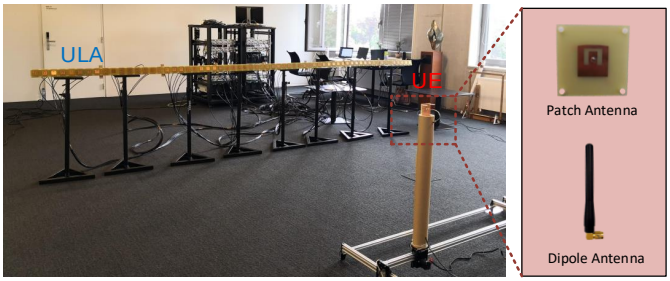

Fig. 2: Indoor localization setup

IV. Measurement and Results

The measurement is based on the massive MIMO testbed at KU Leuven and the measurement scenario is described in Fig. 2. Furthermore, the system runs on the LabVIEW Communications MIMO Application Framework 1.1. The details can be found in [7]. The 64 patch antenna array is deployed at the front of the RF chains in the BS as shown in Fig. 1. On the UE side, we use four XY-tables from Openbuilds ACRO with each side length 1.5 m, to generate the different positions of UEs, and model pedestrian mobility. One USRP-2952 acts as a signal processing unit at the UE, and the transmit antenna is fixed at the mobile robot in the XY-table. The transmit antenna is connected to the USRP-2952 via cable, to create the electromagnetic wavefront.

From the previous study, the antenna type has effects on the angle estimation accuracy. To be specific, as capable of radiating radio power in all directions, the omnidirectional antenna generates more path and results in spurious signals. Intuitively, the multipath effects challenge the estimation accuracy. To verify it, we perform measurement separately with the omnidirectional antenna and the directional antenna as shown in Fig. 2.

In this section, we evaluate the performance of the proposed algorithm by comparing with fourth-order cumulants based on the two-stage MUSIC (TS-MUSIC) algorithm [8], [9], where the oblique projection method is applied for the near-field and far-field source separation. We give the root mean square error (RMSE) of the estimated angle under different SNR and snapshots. The UE will move in one straight line 2.645 m far from the array line. We collect uplink signals from a mobile UE supported by a robot on the XY-tables, which stops every 100 mm, and the robot lingers 30 s at each stop point. In total, 26 positions are measured.

First, In Fig. 3 we plot the RMSE performance in comparison to the number of antennas at the receiver array when the SNR is 10dB, and snapshot $L = 200$. For the measurement scenario as seen in Fig. 2, the far-field condition is satisfied when the number of antennas is less than 6. When considering both near-field and far-field localization, it is observed that the estimation accuracy generally increases with the number of antennas. We conclude that a minimum of 35 antennas is required to achieve an accurate estimation.

In Fig. 4, we plot the RMSE performance versus the SNR

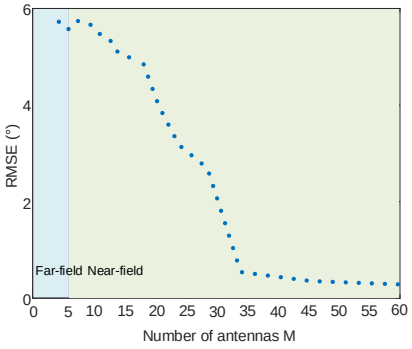

Fig. 3: RMSE performance vs no. antennas (SNR=10 dB, snapshots $L = 200$)

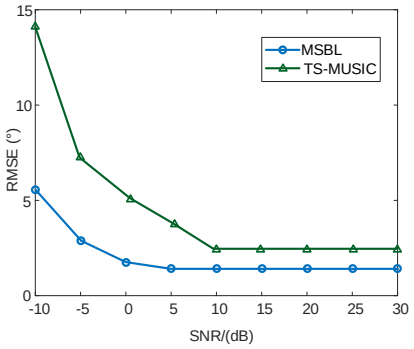

Fig. 4: RMSE performance vs SNR (snapshots $L = 50$)

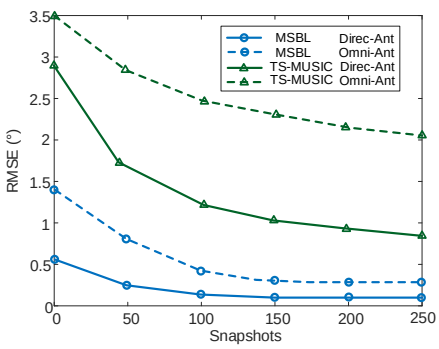

Fig. 5: RMSE performance vs snapshots (SNR= 20 dB)

when snapshots $L = 50$. In the low SNR region (SNR $<$0 dB), the signal subspace and noise subspace in high-order cumulants is correlated, and thus leads to the degradation of TS- MUSIC algorithm performance. When the SNR is low, the noise suppresses the signal sparsity in space, which also accounts for the large estimation errors in the low SNR region. When the SNR $>$ 0 dB, it is observed that the TS-MUSIC performance improves a little, but will enter an error floor, i.e., the increase of SNR (SNR $>$10 dB) can no longer bring a performance improvement. This is due to the TS-MUSIC algorithm that does not consider the phase errors caused by Fresnel approximation, and amplitude errors bought by spherical wave spread, which results in estimation errors for near-field UEs. The proposed MSBL algorithm considers the propagation characteristics of the spherical wavefront and has better performance for the estimation accuracy.

We plot the RMSE performance versus snapshots when SNR $= 20$ dB in Fig. 5. It is observed that the proposed MSBL algorithm reduces 85% RMSE compared with the TS-MUSIC algorithm even when the snapshots L is small ($L = 100$). Recall (27), based on sparse reconstruction, the proposed MSBL algorithm does not involve the inverse of the covariance matrix of the received signals and has robustness even with only a few snapshots. The TS-MUSIC algorithm is a subspace classification method, and cannot avoid the calculation of the inverse of the received signals covariance matrix, which usually is sensitive to the number of snapshots.

Moreover, in Fig. 5, we also show the results that separately evaluated with a directional patch antenna and an omnidirectional dipole antenna at UE. It is observed that, for TS-MUSIC algorithm, 49% reduction in RMSE if applying directional patch antenna instead of omnidirectional dipole antenna at UE when snapshot $L = 100$. A fundamental challenge of indoor localization is the presence of multipath effects. As capable of radiating radio power in all directions, the omnidirectional dipole antenna nevertheless generates more spurious signals. It gives the observation in Fig. 5 that both algorithms achieve better performance with received signals from a directional patch antenna than that from an omnidirectional dipole antenna. Moreover, it is found that, for the proposed MSBL algorithm, the RMSE gap between results from directional patch antenna and an omnidirectional dipole antenna is 0.2° when $L = 100$. Based on sparse reconstruction, the proposed MSBL algorithm does not have extremely rigorous constraints on the signal correlation as the TS-MUSIC algorithm. It thus gives the MSBL algorithm more robustness to multipath effects in the estimation, which explains the narrower performance gap.

V. Conclusion

In this paper we studied the indoor localization in a massive MIMO system with a uniform linear array of 64 antennas. We proposed a mixed field sparse Bayesian learning (MSBL) localization algorithm for both near-field and far-field scenarios. MSBL is robust even with only a few snapshots and in low SNR scenarios. Under the multipath effects, MSBL outperforms other state-of-the-art algorithms. MSBL can also narrow the gap in localization results between using a directional patch antenna and an omnidirectional dipole antenna at the UE. In the future, we will combine a model-based approach in signal processing and a data-driven approach in machine learning, to further improve the localization accuracy.

Acknowledgements

This work was funded by the European Union's Horizon 2020 under grant agreement no. 732174 (ORCA project). B. Liu was supported in part by China Scholarship Council.

References

[1] F. Zafari, A. Gkelias, and K. K. Leung, "A survey of indoor localization systems and technologies," *IEEE Comm. Surveys & Tutorials*, 2019.
[2] N. Garcia, H. Wymeersch, E. Larsson, A. Haimovich, and et al., "Direct localization for massive MIMO," *IEEE Trans. on Signal Process.*, 2017.
[3] J. Lee et al, "A covariance approximation method for near-field direction-finding using a uniform linear array," *IEEE Trans. Signal Process*, 1995.
[4] D. P. Wipf and B. D. Rao, "Sparse bayesian learning for basis selection," *IEEE Transactions on Signal Processing*, pp. 2153–2164, 2004.
[5] P. Gerstoft and et al., "Multisnapshot sparse bayesian learning for DOA," *IEEE Signal Processing Letters*, 2016.
[6] X. Meng and J. Zhu, "A generalized sparse bayesian learning algorithm for 1-bit DOA estimation," *IEEE Communications Letters*, 2018.
[7] C.-M. Chen and et al., "Finite large antenna arrays for massive MIMO: characterization and system impact," *IEEE Trans. on Antennas Propag.*, vol. 65, no. 12, pp. 6712–6720, 2017.
[8] A. Ebrahimi and et al., "Generalised two stage cumulants-based MUSIC algorithm for passive mixed sources localisation," *Signal Process.*, 2019.
[9] X. Zhang and et al., "Localization of near-field sources: A reduced-dimension MUSIC algorithm," *IEEE Communications Letters*, 2018.